Journal of Computational Mathematics
Vol.32, No.1, 2014, 1–20.

http://www.global-sci.org/jcm
doi:10.4208/jcm.1310-m3942

STABILITY FOR IMPOSING ABSORBING BOUNDARY CONDITIONS IN THE FINITE ELEMENT SIMULATION OF ACOUSTIC WAVE PROPAGATION*

Wensheng Zhang
LSEC, ICMSEC, Academy of Mathematics and Systems Science, Chinese Academy of Sciences, Beijing 100190, China
Email: zws@lsec.cc.ac.cn
Eric T. Chung
Department of Mathematics, The Chinese University of Hong Kong, Hong Kong, China
Email: tschung@math.cuhk.edu.hk
Chaowei Wang
ICMSEC, Academy of Mathematics and Systems Science, Chinese Academy of Sciences, Beijing 100190, China
Email: wangcw@lsec.cc.ac.cn

Abstract

It is well-known that artificial boundary conditions are crucial for the efficient and accurate computations of wavefields on unbounded domains. In this paper, we investigate stability analysis for the wave equation coupled with the first and the second order absorbing boundary conditions. The computational scheme is also developed. The approach allows the absorbing boundary conditions to be naturally imposed, which makes it easier for us to construct high order schemes for the absorbing boundary conditions. A third-order Lagrange finite element method with mass lumping is applied to obtain the spatial discretization of the wave equation. The resulting scheme is stable and is very efficient since no matrix inversion is needed at each time step. Moreover, we have shown both abstract and explicit conditional stability results for the fully-discrete schemes. The results are helpful for designing computational parameters in computations. Numerical computations are illustrated to show the efficiency and accuracy of our method. In particular, essentially no boundary reflection is seen at the artificial boundaries.

Mathematics subject classification: 35L05, 35L20, 65M06, 65M12, 65M60.
Key words: Stability, Acoustic wave equation, Simulation, Finite element method, Absorbing boundary conditions, Wave operator decomposition.

1. Introduction

Modeling the propagation of seismic waves is a useful step in the interpretation of wave phenomena in complex media. It is also an essential step for inverse problem in seismic exploration. Several kinds of techniques for wave modeling have been developed. These include the finite volume method ([13, 49]), the finite difference method ([2, 20, 32, 43, 52, 53]), the spectral method ([6, 30, 31]), the spectral element method ([28, 29]), the finite element method ([17, 18, 33]) and the discontinuous Galerkin methods ([9, 10, 12, 14, 15]).

The finite difference method is a popular numerical technique because it is relatively easy to implement and has high computational efficiency. The wave modeling with the finite difference

* Received November 18, 2011 / Revised version received July 25, 2013 / Accepted October 9, 2013 / Published online January 22, 2014 /

method in seismology was realized early in 70s ([2]). Since then, various finite difference schemes for wave modeling are proposed. For example, Dablain [20] proposed the high-order difference schemes. Virieux [43] investigated the stagger-grid difference scheme which has some advantages in physical aspects. Sei [36] generalized a family of high order finite difference schemes for the computation of elastic waves. Zhang et al. [52] proposed a new high accuracy locally one-dimensional scheme for the wave equation. The spectral element method was introduced firstly in computational fluid dynamic ([35]). It have been successfully applied to seismic wave simulation ([28, 29]). However, its computational mesh is usually quadrilateral grid in 2D case or hexahedral in 3D case.

The finite element method (FEM) especially the triangular element has a distinctive advantage of being able to handle problems with complex domains. Thus, the FEM has a potential and room for development in seismic wave simulations. However, the high order FEM is still not widely used in the simulation of seismic waves and the main reason is that it requires the inversion of the mass matrix at each extrapolation time step. This implies that the FEM has very low computational efficiency especially when many extrapolation time steps are required. The advantage of FEM is its good adaptability to various velocity models with high complexity. Finite elements with simplices fit better the polygonal shaped domains and sharp contrasts in velocity models. The FEM requires the solution of a large sparse linear system of equations, which makes the method costly. This cost can be avoided by mass lumping ([54]), a technique that replaces the large linear system by a diagonal matrix. For the low order methods such as the linear Lagrange element, the mass lumping can be implemented by using the quadratic rules for numerical integration. But it is not obvious how mass lumping is implemented for high order methods such as the quadratic Lagrange element. As high order accuracy is desired in wave simulation, we will adopt the third-order Lagrange element in our computations which preserves the accuracy and at the same time allows mass lumping ([17, 18]).

In numerical simulation of wave propagation, the imposition of artificial boundary introduces spurious reflections which will devastate the accuracy of numerical solutions. Although the problem can be overcome by increasing the size of the computational domain, it is not always feasible because it increases the amount of computations. In order to eliminate the boundary reflections, absorbing boundary conditions are desirable in wave modeling. There are several kinds of absorbing boundary conditions (ABCs) (see e.g., [5, 7, 14–16, 22, 25, 26, 37]). Smith [37] proposed a nonreflection plane boundary, which is easily implemented for finite difference and finite element calculations. Clayton and Engquist [16] proposed the ABCs based on the paraxial approximations of the acoustic or elastic equations. Another approach is to add damping layer to the boundaries ([7]). The waves entering this damping layer will be absorbed. The perfectly matched layer (PML) method is based on the use of an absorbing layer especially designed to absorb without reflection waves ([5]). These ABCs have been widely used in the finite difference method. Chung (et al., [14, 15]) considered the ABCs in wave simulation with the optimal discontinuous Galerkin methods. In this paper, we focus on stability analysis for implementing the ABCs with the high order Lagrange finite element. The computational scheme is also developed. The ABCs based on the factorization of wave equation are reviewed and the variational framework, which imposes the ABCs weakly, is derived. The spatial discretization of the weak form of wave equation including the embedded boundary conditions has high spatial accuracy. Moreover, we obtain and prove new abstract and explicit stability conditions for the proposed computational scheme.

2. Theory

2.1. Weak formulation with Dirichlet boundary condition

In this subsection, we will briefly state the variational form of the wave equation with the Dirichlet boundary condition to introduce our notations. We consider the following 2-D acoustic wave problem

$$\frac{1}{c(x,z)^2}\frac{\partial^2 u}{\partial t^2} - \frac{\partial^2 u}{\partial x^2} - \frac{\partial^2 u}{\partial z^2} = 0, \qquad (x,z) \in \Omega,\ t > 0, \tag{2.1}$$

$$u(x,z,0) = g_1(x,z), \quad \frac{\partial u(x,z,0)}{\partial t} = g_2(x,z), \quad (x,z) \in \Omega, \tag{2.2}$$

$$u(x,z,t)|_{\partial\Omega} = 0, \qquad t > 0, \tag{2.3}$$

where Ω denotes a bounded polygonal subset of $\mathbb{R}^2$ with boundary $\partial\Omega$.

In the above system $u(x,z,t)$ is the unknown wavefield and $c(x,z)$ is the given velocity of the medium. Let V_h be an approximation subspace spanned by the Lagrange finite element functions. To get the weak formulation of the acoustic wave equation, we multiply (2.1) by a test function $v(x,z) \in V_h$ and integrate over the domain Ω and apply the Green's first identity

$$\iint_\Omega \varphi(\frac{\partial^2 \phi}{\partial x^2} + \frac{\partial^2 \phi}{\partial z^2})dxdz = -\iint_\Omega \nabla\varphi \cdot \nabla\phi dxdz + \oint_{\partial\Omega} \varphi \frac{\partial \phi}{\partial \boldsymbol{n}} ds, \tag{2.4}$$

where φ and ϕ are the continuously differentiable functions, $\boldsymbol{n}$ is the outward pointing unit normal of domain boundary, ∇ is the gradient operator. As a result, we have

$$\begin{aligned}\frac{d^2}{dt^2}\iint_\Omega \frac{1}{c^2(x,z)} u(x,z,t)v(x,z)dxdz \\ + \iint_\Omega \nabla u(x,z,t)\cdot\nabla v(x,z)dxdz - \int_{\partial\Omega} \frac{\partial u(x,z,t)}{\partial n} v(x,z)ds = 0, \quad \forall v \in V_h.\end{aligned} \tag{2.5}$$

Considering the Dirichlet condition or $v|_{\partial\Omega} = 0$, we have the weak formulation

$$\begin{aligned}\frac{d^2}{dt^2}\iint_\Omega \frac{1}{c^2(x,z)} u(x,z,t)v(x,z)dxdz \\ + \iint_\Omega \nabla u(x,z,t)\cdot\nabla v(x,z)dxdz = 0, \quad \forall v \in V_h.\end{aligned} \tag{2.6}$$

Let w_i be the corresponding Lagrange basis of V_h. Thus we can express $u_h = \sum \alpha_i(t) w_i$. We define $U(t)$ to be the vector consists of the coefficients α_i. Then (2.6) is equivalent to the following ordinary differential system

$$M\frac{d^2U(t)}{dt^2} + KU(t) = 0, \tag{2.7}$$

where the mass matrix M and the stiffness matrix K are given respectively by

$$M_{ij} = \iint_\Omega \frac{1}{c^2(x,z)} w_i(x,z)w_j(x,z)dxdz, \tag{2.8}$$

$$K_{ij} = \iint_\Omega \nabla w_i(x,z)\cdot\nabla w_j(x,z)dxdz. \tag{2.9}$$

In computations, we need to select a suitable finite element space. In the case of P_1 Lagrange element, the following trapezoidal quadrature rule is used

$$\iint_{\Delta A_1A_2A_3} f(x,z)dxdz = \frac{1}{3}|\Delta A_1A_2A_3|\Big[f(A_1)+f(A_2)+f(A_3)\Big], \tag{2.10}$$

where $f(x,z)$ is a given function, and $|\Delta A_1A_2A_3|$ denotes the area of the triangle $\Delta A_1A_2A_3$ shown in Fig. 2.1. For the linear element, the approximate mass matrix is diagonal. However, for high order elements, such as P_2 element which shown in Fig. 2.1(a), the approximate mass matrix is not diagonal. As the mass matrix must be inverted at each time step, the mass lumping technique is required to improve computational efficiency. Here, we adopt the third-order Lagrange element of [17]. It extends P_2 to $\tilde{P}_2$ by $\tilde{P}_2 = P_2 \oplus \lambda_1\lambda_2\lambda_3$, where $\lambda_1\lambda_2\lambda_3$ is the bubble function, and $\lambda_1, \lambda_2, \lambda_3$ are the baycentric coordinates with respect to vertices A_1, A_2, A_3 of the triangle $\Delta A_1A_2A_3$. Here $\oplus$ denotes direct sum. Obviously, the space $\tilde{P}_2$ satisfies $P_2 \subset \tilde{P}_2 \subset P_3$ and ensures the H^1 conforming nature of V_h on the element boundary. Then by using the following quadrature formula

$$\begin{aligned}\iint_{\Delta A_1A_2A_3} f(x,z)dxdz = |\Delta A_1A_2A_3|\Big(&\frac{1}{20}[f(A_1)+f(A_2)+f(A_3)]\\ &+\frac{2}{15}[f(M_1)+f(M_2)+f(M_3)]+\frac{9}{20}f(G)\Big),\end{aligned} \tag{2.11}$$

the mass matrix keeps diagonal. This quadrature formula is exact in P_3 and the weights in it are strictly positive. The seven interpolation nodes used on the triangle $\Delta A_1A_2A_3$ are shown in Fig. 2.1 (b). For the boundary integrals, for instances the boundary integral along the edge $\overline{A_1A_2}$, the following Simpson rule ([1])

$$\int_{\overline{A_1A_2}} f(x,z)ds = \frac{1}{6}|\overline{A_1A_2}|\Big(f(A_1)+4f(M_3)+f(A_2)\Big), \quad (x,z)\in\overline{A_1A_2}, \tag{2.12}$$

is used which has local truncation error with third-order accuracy in space and keeps the mass lumping feature. Here $|\overline{A_1A_2}|$ is the length of edge $\overline{A_1A_2}$. The theoretical analysis for $\tilde{P}_2$ such as the convergence and error estimates can be found in [17].

2.2. Absorbing boundary conditions derived from wave operator decomposition

Absorbing boundary conditions make a numerical computation of the solution in the bounded domain behave as the computational boundary were not present. The development of stable and effective ABCs is an important issue in numerical modeling. Substantial work has been performed on such problems (see, e.g., [5, 7, 16, 19, 22, 25, 26]). Here we derive ABCs based on the idea of wave operator decomposition ([47]). The method of wave operator decomposition has been extended and applied to wave equation migration/inversion in [48, 51]. The obtained ABCs are essentially the Clayton and Engquist's ABCs when the leading terms are kept in decomposition.

As shown is Fig. 2.2, the computational domain Ω is a rectangle, and $\partial\Omega$ consists of four parts named Γ_1, Γ_2, Γ_3 and Γ_4. Assume the positive direction of x and z is right and down respectively. We factorize the 1-D wave equation in the following form

$$\Big(\frac{1}{c}\frac{\partial}{\partial t}-\frac{\partial}{\partial x}\Big)\Big(\frac{1}{c}\frac{\partial}{\partial t}+\frac{\partial}{\partial x}\Big)u = 0. \tag{2.13}$$

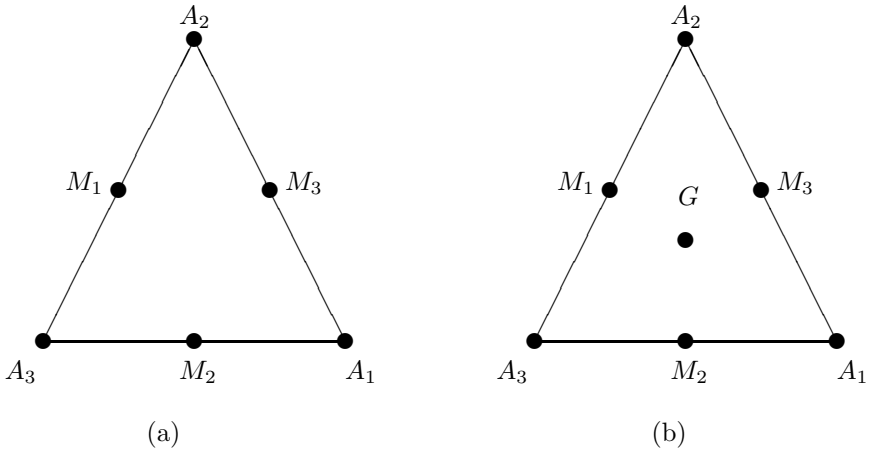

Fig. 2.1. Two nodes distribution for the third-order Lagrange element. (a) Six interpolation nodes on a triangular element. This element makes the approximate mass matrix be not diagonal; (b) Seven interpolation nodes on a triangular element. The nodes consist of three vertices A_1, A_2 and A_3, three midpoints M_1, M_2 and M_3 and the centroid G. The element makes the approximate mass matrix be diagonal.

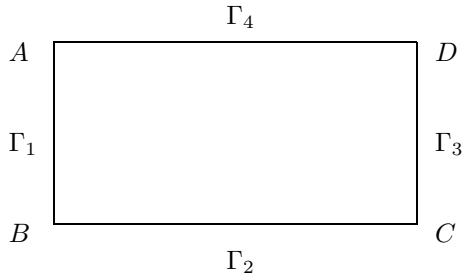

Fig. 2.2. Domain Ω for wave simulation. Its boundary $\partial\Omega$ consists of four sides denoted by Γ_1, Γ_2, Γ_3 and Γ_4 respectively. The positive directions of x and z point to right and down respectively.

Then we define the rightgoing wave R and leftgoing wave L by

$$R = \Big(\frac{1}{c}\frac{\partial}{\partial t} - \frac{\partial}{\partial x}\Big)u, \tag{2.14}$$

$$L = \Big(\frac{1}{c}\frac{\partial}{\partial t} + \frac{\partial}{\partial x}\Big)u, \tag{2.15}$$

respectively. One wants outgoing wave motions should pass through the boundary without being reflected. Therefore the outgoing waves R and L should satisfy

$$\frac{1}{c}\frac{\partial R}{\partial t} + \frac{\partial R}{\partial x} = 0, \qquad x \in \Gamma_3, \tag{2.16}$$

$$\frac{1}{c}\frac{\partial L}{\partial t} - \frac{\partial L}{\partial x} = 0, \qquad x \in \Gamma_1, \tag{2.17}$$

respectively. They are the first-order ABCs for the left boundary Γ_1 and right boundary Γ_3 respectively. Similarly defining the downgoing wave D and upgoing wave U, we can obtain the

first-order ABCs for the bottom boundary Γ_2 and the top boundary Γ_1:

$$\frac{1}{c}\frac{\partial D}{\partial t}+\frac{\partial D}{\partial z}=0, \qquad x\in\Gamma_2, \tag{2.18}$$

$$\frac{1}{c}\frac{\partial U}{\partial t}-\frac{\partial U}{\partial z}=0, \qquad x\in\Gamma_4. \tag{2.19}$$

We point out that the downgoing and upgoing wave equations (2.18)-(2.19) are the simplified forms of the following coupled equations ([47])

$$\frac{1}{c}\frac{\partial D}{\partial t}+\frac{\partial D}{\partial z}=-\frac{\partial c}{2c\partial z}(D+U), \quad x\in\Gamma_2, \tag{2.20}$$

$$\frac{1}{c}\frac{\partial U}{\partial t}-\frac{\partial U}{\partial z}=\frac{\partial c}{2c\partial z}(D+U), \qquad x\in\Gamma_4. \tag{2.21}$$

We remark that for simplicity we only consider the completely decoupled form of downgoing wave and upcoming wave. From the physical point of view, that is to say, we don't consider the effects of multiple waves and true-amplitude preserving. The general coupled expression of the 3D wave operator decomposition can be found in the reference [47].

The high order one-wave equations or ABCs can also be obtained by some ways ([25, 26, 46]). The nth order ABC for Γ_3 is

$$\Big(\frac{1}{c}\frac{\partial}{\partial t}+\frac{\partial}{\partial x}\Big)^n u=0, \qquad x\in\Gamma_3, \tag{2.22}$$

where u denotes any one-way wave for simplicity. Setting $n=2$ and noting that u is also the solution of wave equation (2.1), we obtain the second-order ABC for Γ_1

$$\frac{\partial^2 u}{\partial t^2}-c\frac{\partial^2 u}{\partial x\partial t}-\frac{c^2}{2}\frac{\partial^2 u}{\partial z^2}=0, \qquad (x,z)\in\Gamma_1. \tag{2.23}$$

Similarly, we can obtain the second-order ABCs for Γ_3, Γ_2 and Γ_4 respectively:

$$\frac{\partial^2 u}{\partial t^2}+c\frac{\partial^2 u}{\partial x\partial t}-\frac{c^2}{2}\frac{\partial^2 u}{\partial z^2}=0, \qquad (x,z)\in\Gamma_3, \tag{2.24}$$

$$\frac{\partial^2 u}{\partial t^2}+c\frac{\partial^2 u}{\partial z\partial t}-\frac{c^2}{2}\frac{\partial^2 u}{\partial x^2}=0, \qquad (x,z)\in\Gamma_2, \tag{2.25}$$

$$\frac{\partial^2 u}{\partial t^2}-c\frac{\partial^2 u}{\partial z\partial t}-\frac{c^2}{2}\frac{\partial^2 u}{\partial x^2}=0, \qquad (x,z)\in\Gamma_4. \tag{2.26}$$

In order to consider the absorbing effects, we consider the reflection coefficient which is defined as the ratio of the reflected wavefield to an incident plane wave. Insert into (2.22) a linear combination of an incoming wave $e^{i(x\cos\theta+z\sin\theta-ct)}$ and an outgoing wave $e^{i(-x\cos\theta+z\sin\theta-ct)}$ to get the reflection coefficient

$$|R_n|=\Big(\frac{1-\cos\theta}{1+\cos\theta}\Big)^n, \tag{2.27}$$

where θ is the angle of incidence. Based on the theory of wave reflection ([3]), if one wants to annihilate waves moving with angle α, the version corresponding to (2.27) becomes

$$|R_n|=\Big(\frac{\cos\alpha-\cos\theta}{\cos\alpha+\cos\theta}\Big)^n. \tag{2.28}$$

The magnitude of the reflection coefficient is plotted as a function of incidence angles θ in Fig. 2.3 for four different absorbtion directions: 0°, 15°, 30° and 45°. The solid line indicates the

first-order ABCs ($n = 1$) and the dotted line the second-order ABCs ($n = 2$). Fig. 2.3(a) and 2.3(b) show that the magnitude of the reflection coefficients of first-order ABCs is small for 0° and 15° absorbtion directions, while it becomes large in Fig. 2.3(c) and 2.3(d) for 30° and 45° absorbtion directions. For the second-order ABCs, the reflection magnitude is even small for the 45° absorbtion direction. Obviously, the effectively absorbing angle of the second-order ABCs is lager than that of the first-order ABCs.

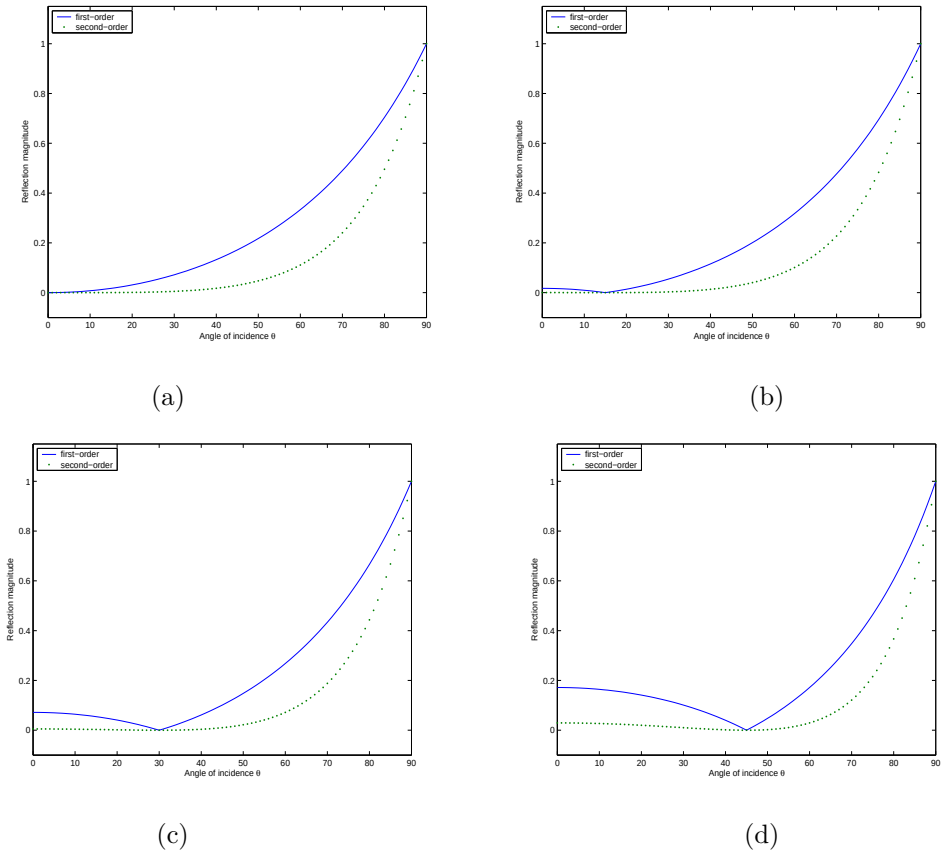

Fig. 2.3. A comparison of reflection coefficient magnitude between the first-order (solid) and second-order (dotted) ABCs for four different absorption directions: (a) 0°, (b) 15°, (c) 30° and (d) 45°.

2.3. Wavefield extrapolation schemes with absorbing boundary conditions

In this subsection, we will derive the variational form and the discretization schemes for the wave equation which imposes the absorbing boundary conditions naturally. Since $v|_{\partial\Omega} \neq 0$, the third term of LHS in (2.5) is not zero. Notice that the first-order ABCs (2.16)-(2.19) can be written as

$$\frac{\partial u}{\partial \boldsymbol{n}} + \frac{1}{c}\frac{\partial u}{\partial t} = 0, \quad (x, z) \in \partial\Omega. \tag{2.29}$$

Substituting (2.29) in (2.5) yields the weak formulation (2.30) for the first-order ABCs: find $u_h \in V_h$ such that

$$\frac{d^2}{dt^2}\iint_\Omega \frac{1}{c^2} u_h v_h dxdz + \iint_\Omega \nabla u_h \cdot \nabla v_h dxdz + \int_{\partial\Omega} \frac{1}{c} u_h v_h ds = 0, \quad \forall v_h \in V_h. \tag{2.30}$$

We note that the ABCs are naturally incorporated into the weak formulation by the term $\int_{\partial\Omega}\frac{1}{c}u_hv_hds$. Using the central difference scheme for the time derivative, the discretization scheme of (2.30) for wavefield extrapolation can be written as

$$(2M+L\Delta t)U^{n+1}+(2\Delta t^2K-4M)U^n+(2M-L\Delta t)U^{n-1}=0, \tag{2.31}$$

where $U^n(t)=U(n\Delta t)$, and L is the matrix given by

$$L_{ij}=\int_{\partial\Omega}\frac{1}{c}w_iw_jds. \tag{2.32}$$

We note that L is a symmetric positive-definite matrix.

For the second-order ABCs, first taking time derivative on both sides of (2.5), we obtain

$$\frac{d^3}{dt^3}\iint_\Omega\frac{1}{c^2}uvdxdz+\frac{d}{dt}\iint_\Omega\nabla u\cdot\nabla vdxdz-\int_{\partial\Omega}\frac{\partial^2u}{\partial\boldsymbol{n}\partial t}vds=0. \tag{2.33}$$

Then we compute the boundary integral in (2.33) in the following way

$$\begin{aligned}
-\int_{\partial\Omega}\frac{\partial^2u}{\partial\boldsymbol{n}\partial t}vds&=-\int_{\Gamma_1}\frac{\partial^2u}{\partial\boldsymbol{n}\partial t}vds-\int_{\Gamma_2}\frac{\partial^2u}{\partial\boldsymbol{n}\partial t}vds-\int_{\Gamma_3}\frac{\partial^2u}{\partial\boldsymbol{n}\partial t}vds-\int_{\Gamma_4}\frac{\partial^2u}{\partial\boldsymbol{n}\partial t}vds\\
&=-\int_{\Gamma_1}\Big(\frac{c}{2}\frac{\partial^2u}{\partial z^2}-\frac{1}{c}\frac{\partial^2u}{\partial^2t}\Big)vdz-\int_{\Gamma_2}\Big(\frac{c}{2}\frac{\partial^2u}{\partial x^2}-\frac{1}{c}\frac{\partial^2u}{\partial^2t}\Big)vdx\\
&\quad-\int_{\Gamma_3}\Big(\frac{c}{2}\frac{\partial^2u}{\partial z^2}-\frac{1}{c}\frac{\partial^2u}{\partial^2t}\Big)vdz-\int_{\Gamma_4}\Big(\frac{c}{2}\frac{\partial^2u}{\partial x^2}-\frac{1}{c}\frac{\partial^2u}{\partial^2t}\Big)vdx\\
&=\frac{d^2}{dt^2}\int_{\partial\Omega}\frac{1}{c}uvds+\frac{c}{2}\Big[\int_{\Gamma_1}\frac{\partial u}{\partial z}\frac{\partial v}{\partial z}dz+\int_{\Gamma_3}\frac{\partial u}{\partial z}\frac{\partial v}{\partial z}dz\\
&\quad+\int_{\Gamma_2}\frac{\partial u}{\partial x}\frac{\partial v}{\partial x}dx+\int_{\Gamma_4}\frac{\partial u}{\partial x}\frac{\partial v}{\partial x}dx\Big]\\
&=\frac{d^2}{dt^2}\int_{\partial\Omega}\frac{1}{c}uvds+\frac{c}{2}\Big[\int_{\Gamma_1+\Gamma_3}\frac{\partial u}{\partial z}\frac{\partial v}{\partial z}dz+\int_{\Gamma_2+\Gamma_4}\frac{\partial u}{\partial x}\frac{\partial v}{\partial x}dx\Big].
\end{aligned}\tag{2.34}$$

Substituting the above result in (2.33), we obtain the variational form

$$\begin{aligned}
&\frac{d^3}{dt^3}\iint_\Omega\frac{1}{c^2}uvdxdz+\frac{d}{dt}\iint_\Omega\nabla u\cdot\nabla vdxdz\\
&\quad+\frac{d^2}{dt^2}\int_{\partial\Omega}\frac{1}{c}uvds+\frac{c}{2}\int_{\Gamma_1+\Gamma_3}\frac{\partial u}{\partial z}\frac{\partial v}{\partial z}dz+\frac{c}{2}\int_{\Gamma_2+\Gamma_4}\frac{\partial u}{\partial x}\frac{\partial v}{\partial x}dx=0.
\end{aligned}\tag{2.35}$$

Thus the variational form with the second-order ABCs reads: find $u_h\in V_h$ such that

$$\begin{aligned}
&\frac{d^3}{dt^3}\iint_\Omega\frac{1}{c^2}u_hv_hdxdz+\frac{d}{dt}\iint_\Omega\nabla u_h\cdot\nabla v_hdxdz\\
&\quad+\frac{d^2}{dt^2}\int_{\partial\Omega}\frac{1}{c}u_hv_hds+\frac{c}{2}\int_{\Gamma_1+\Gamma_3}\frac{\partial u_h}{\partial z}\frac{\partial v_h}{\partial z}dz+\frac{c}{2}\int_{\Gamma_2+\Gamma_4}\frac{\partial u_h}{\partial x}\frac{\partial v_h}{\partial x}dx=0.
\end{aligned}\tag{2.36}$$

Now we propose to approximate the derivatives with respect to time t in (2.36) with the

following expressions

$$\frac{d^3u}{dt^3} = \frac{u^{n+2} + 2u^{n-1} - 2u^{n+1} - u^{n-2}}{2\triangle t^3} + O(\triangle t^2), \tag{2.37}$$

$$\frac{d^2u}{dt^2} = \frac{u^{n+2} - 2u^n + u^{n-2}}{4\triangle t^2} + O(\triangle t^2), \tag{2.38}$$

$$\frac{du}{dt} = \frac{u^{n+1} - u^{n-1}}{2\triangle t} + O(\triangle t^2). \tag{2.39}$$

Then the wavefield extrapolation scheme with the second-order ABCs (2.36) can be written as

$$\begin{aligned}(2M + L\Delta t)U^{n+2} + (2K\Delta t^2 - 4M)U^{n+1} + (4\Delta t^3 J - 2L\Delta t)U^n \\ +(4M - 2K\Delta t^2)U^{n-1} + (L\Delta t - 2M)U^{n-2} = 0,\end{aligned} \tag{2.40}$$

where L is given by (2.32) and J is the matrix given by

$$(J)_{ij} = \frac{c}{2}\int_{\Gamma_1+\Gamma_3} \frac{\partial w_i}{\partial z}\frac{\partial w_j}{\partial z}dz + \frac{c}{2}\int_{\Gamma_2+\Gamma_4} \frac{\partial w_i}{\partial x}\frac{\partial w_j}{\partial x}dx. \tag{2.41}$$

One notes that J is the symmetric positive semi-definite matrix.

3. Stability Conditions

3.1. General formulation

New stability conditions for the fully-discrete schemes (2.31) and (2.40) with the first-order and second-order ABCs respectively are derived here. First, we consider the wavefield extrapolation using (2.7) for the Dirichlet boundary condition. Its discretization scheme is

$$\frac{U^{n+1} - 2U^n + U^{n-1}}{\Delta t^2} + M^{-1}KU^n = 0. \tag{3.1}$$

The difference equations both for the Dirichlet condition and the first-order ABCs can be written as

$$B_2U^{n+1} + B_1U^n + B_0U^{n-1} = 0, \tag{3.2}$$

where B_0, B_1 and B_2 are linear combinations of M, K and L. For the case with the Dirichlet condition, we have

$$B_2 = I, \quad B_1 = \Delta t^2 M^{-1}K - 2, \quad B_0 = I, \tag{3.3}$$

where I is the identity matrix, while for the case with the first-order ABCs, we have

$$B_2 = 2M - \Delta tL, \quad B_1 = 2\Delta t^2 K - 4M, \quad B_0 = 2M + \Delta tL. \tag{3.4}$$

Eq. (3.2) has the characteristic polynomial

$$Q_2(r) \equiv det\{B_2r^2 + B_1r + B_0\}, \tag{3.5}$$

and when we apply the appropriate transform $r = \frac{1+z}{1-z}$ which maps the interior of the circle $|r| = 1$ into the half-plane $Rez < 0$, we obtain the eigenproblem

$$P_2(z)\boldsymbol{s} \equiv \Big(A_2z^2 + A_1z + A_0\Big)\boldsymbol{s} = \mathbf{0}, \tag{3.6}$$

where

$$A_2 = B_2 - B_1 + B_0, \quad A_1 = 2(B_2 - B_0), \quad A_0 = B_2 + B_1 + B_0. \tag{3.7}$$

For the case with the Dirichlet condition, the matrices in (3.6) are defined as

$$A_2 = 4I - \Delta t^2 M^{-1} K, \quad A_1 = 0, \quad A_0 = \Delta t^2 M^{-1} K, \tag{3.8}$$

and for the case with the first-order ABCs, the matrices in (3.6) are defined as

$$A_2 = 8M - 2\Delta t^2 K, \quad A_1 = 4\Delta t L, \quad A_0 = 2\Delta t^2 K. \tag{3.9}$$

Since A_0 and A_1 are clearly positive semi-definite in both (3.8) and (3.9), A_2 being positive definite is sufficient to guarantee stability. Thus we have the result that a sufficient condition for stability is $\Delta t < 2\sqrt{1/\lambda}$, where λ is the eigenvalue of $M^{-1}K$. After taking minimization over all eigenvalues, we obtain the stability condition for the scheme with the Dirichlet condition and first-order ABCs

$$\Delta t < \min\Big\{2\sqrt{\frac{1}{\lambda}}\Big\}, \tag{3.10}$$

where λ is the eigenvalue of $M^{-1}K$.

For the case with the second-order ABCs, its difference matrix equation can be written as

$$B_4 U^{n+2} + B_3 U^{n+1} + B_2 U^n + B_1 U^{n-1} + B_0 U^{n-2} = 0, \tag{3.11}$$

where

$$\begin{array}{lll} B_4 = 2M + \Delta t L, & B_3 = 2\Delta t^2 K - 4M, & \\ B_2 = 4\Delta t^3 J - 2\Delta t L, & B_1 = 4M - 2\Delta t^2 K, & B_0 = \Delta t L - 2M. \end{array} \tag{3.12}$$

Similarly, we obtain the corresponding eigenproblem

$$P_4(z)\boldsymbol{s} \equiv \Big(A_4 z^4 + A_3 z^3 + A_2 z^2 + A_1 z^1 + A_0 z^0\Big)\boldsymbol{s} = \mathbf{0}, \tag{3.13}$$

where

$$\begin{array}{l} A_4 = B_4 - B_3 + B_2 - B_1 + B_0 = 4\Delta t^3 J, \\ A_3 = 4B_4 - 2B_3 + 2B_1 - 4B_0 = 24M - 8\Delta t^2 K, \\ A_2 = 6B_4 - 2B_2 + 6B_0 = 16\Delta t L - 8\Delta t^3 J, \\ A_1 = 4B_4 + 2B_3 - 2B_1 - 4B_0 = 8\Delta t^2 K, \\ A_0 = B_4 + B_3 + B_2 + B_1 + B_0 = 0. \end{array} \tag{3.14}$$

Necessary conditions for stability are that the matrices $A_i (i = 0, 1, 2, 3, 4)$ are positive semi-definitive, which yields $\Delta t < \sqrt{3/\lambda}$ from A_3 and $\Delta t < \sqrt{2/\mu}$ from A_2, where μ is the eigenvalue of matrix $L^{-1}J$. Therefore, the necessary stability condition for the scheme with the second-order ABCs is

$$\Delta t < \min\Big\{\sqrt{\frac{3}{\lambda}}, \sqrt{\frac{2}{\mu}}\Big\} \tag{3.15}$$

where λ and μ are the eigenvalues of matrices $M^{-1}K$ and $L^{-1}J$ respectively. Combing the results above, we have the following theorem:

Theorem 3.1. *The necessary stability condition is*

$$\Delta t < \min\Big\{2\sqrt{\frac{1}{\lambda}}\Big\}, \tag{3.16}$$

for the Dirichlet condition and first-order ABCs, and is

$$\Delta t < \min\Big\{\sqrt{\frac{3}{\lambda}}, \sqrt{\frac{2}{\mu}}\Big\}, \tag{3.17}$$

for the second-order ABCs, where λ and μ are the eigenvalues of matrices $M^{-1}K$ and $L^{-1}J$ respectively.

3.2. Explicit expressions

Usually, the resulting stiffness matrix or mass matrix from the finite element spatial discretization is large. Estimating the Δt from (3.16) or (3.17) by calculating eigenvalue λ or μ is not easy for large-scale matrix. In this subsection, we will derive the explicit expressions based on the mesh information which are easy to be applied in computations. The condition number of the stiffness matrix resulting from the finite element discretization is an important problem. Actually this problem has been a constant research topic for many decades, for example, see [4, 21, 23, 24, 27, 34, 38, 44]. In the following we propose to estimate the Δt by computing the corresponding matrices on the element. The used finite element in discretization is the third-order Lagrange element introduced in Section 2.1. The method developed here can be used for other high order elements without essential difficulty. The computations are usually implemented in the reference element shown in Fig. 3.1. A affine transformation may be used in computations to map $\Delta A_1A_2A_3$ in Fig. 2.1(b) to the reference element $\tilde{\mathcal{K}}$ in Fig. 3.1 (see, e.g., [28, 45, 54]). The seven basis functions at the three vertices $\hat{S}_1, \hat{S}_2, \hat{S}_3$, three midpoints $\hat{M}_1, \hat{M}_2, \hat{M}_3$ and the centroid $\hat{G}$ are

$$\begin{aligned}
\hat{S}_1 :&\quad 2\lambda_1^2 - \lambda_1 + 3\lambda_1\lambda_2\lambda_3,\\
\hat{S}_2 :&\quad 2\lambda_2^2 - \lambda_2 + 3\lambda_1\lambda_2\lambda_3,\\
\hat{S}_3 :&\quad 2\lambda_3^2 - \lambda_3 + 3\lambda_1\lambda_2\lambda_3,\\
\hat{M}_1 :&\quad 4\lambda_2\lambda_3 - 12\lambda_1\lambda_2\lambda_3,\\
\hat{M}_2 :&\quad 4\lambda_1\lambda_3 - 12\lambda_1\lambda_2\lambda_3,\\
\hat{M}_3 :&\quad 4\lambda_1\lambda_2 - 12\lambda_1\lambda_2\lambda_3,\\
\hat{G} :&\quad 27\lambda_1\lambda_2\lambda_3,
\end{aligned} \tag{3.18}$$

respectively, where λ_1, λ_2 and λ_3 are the barycentre coordinates and $\lambda_1 + \lambda_2 + \lambda_3 = 1$.

To start with, we consider the element mass matrix M on the reference element $\hat{\mathcal{K}}$. For convenience, we omit the velocity in the matrices M and L in the derivation and add it in the final result. After calculating by (2.8) and (2.11) we know the expression of the element mass matrix $\hat{M}$ is a 7×7 diagonal matrix with the diagonal elements:

$$diag\Big(\frac{1}{40}, \frac{1}{40}, \frac{1}{40}, \frac{1}{15}, \frac{1}{15}, \frac{1}{40}, \frac{9}{40}\Big). \tag{3.19}$$

Notice that M is a diagonal matrix. It it obvious that

$$\lambda(M) \geqslant \min_j M_{jj}. \tag{3.20}$$

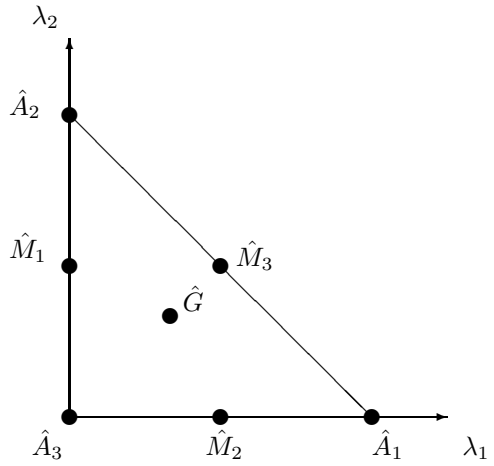

Fig. 3.1. The reference triangular element $\tilde{\mathcal{K}}$ in the Cartesian coordinate system $\lambda_1 - \lambda_2$.

For the mesh with the right-angle side h shown in Fig. 3.2, we have

$$\lambda(M) \geqslant \frac{2}{15}. \tag{3.21}$$

The stiff matrix K on the reference element $\hat{\mathcal{K}}$ is given by

$$\hat{K} = \begin{bmatrix} \frac{2}{5} & -\frac{1}{10} & -\frac{1}{30} & \frac{1}{5} & -\frac{7}{15} & 0 & 0 \\ -\frac{1}{10} & \frac{2}{5} & -\frac{1}{30} & -\frac{7}{15} & \frac{1}{5} & 0 & 0 \\ -\frac{1}{30} & -\frac{1}{30} & \frac{7}{10} & -\frac{1}{15} & -\frac{1}{15} & \frac{2}{5} & -\frac{9}{10} \\ \frac{1}{5} & -\frac{7}{15} & -\frac{1}{15} & \frac{8}{3} & 0 & -\frac{8}{15} & -\frac{9}{5} \\ -\frac{7}{15} & \frac{1}{5} & -\frac{1}{15} & 0 & \frac{8}{3} & -\frac{8}{15} & -\frac{9}{5} \\ 0 & 0 & \frac{2}{5} & -\frac{8}{15} & -\frac{8}{15} & \frac{64}{15} & -\frac{18}{5} \\ 0 & 0 & -\frac{9}{10} & -\frac{9}{5} & -\frac{9}{5} & -\frac{18}{5} & \frac{81}{10} \end{bmatrix}, \tag{3.22}$$

and the maximal eigenvalue of $\hat{K}$ is $\lambda_{max}(\hat{K}) = 10.773929$. We estimate the upper bound estimation of the eigenvalues of the stiff matrix K. Let $\hat{K}$ be the element stiff matrix on the reference element. And let $\boldsymbol{u}_k$ be the restriction of vector $\boldsymbol{u}$ on $\mathcal{K}$. Then

$$\begin{aligned} \boldsymbol{u}^T K \boldsymbol{u} &= \sum_{\mathcal{K}\in\tau_h} \iint_{\mathcal{K}} \nabla w_i \nabla w_j dxdz = \sum_{\mathcal{K}\in\tau_h} \boldsymbol{u}_{\mathcal{K}}^T \hat{K} \boldsymbol{u}_{\mathcal{K}} \\ &\leqslant \lambda_{max}(\hat{K}) \sum_{\mathcal{K}\in\tau_h} ||\boldsymbol{u}_{\mathcal{K}}||_0^2 = \lambda_{max}(\hat{K}) \sum_{\mathcal{K}\in\omega_j} ||\boldsymbol{u}_{\mathcal{K}}||_0^2 \\ &\leqslant \lambda_{max}(\hat{K}) \max \aleph_{\omega_j} \boldsymbol{u}^T \boldsymbol{u}, \end{aligned} \tag{3.23}$$

Thus we have

$$\lambda(K) \leqslant \lambda_{max}(\hat{K}) \max \aleph_{\omega_j}. \tag{3.24}$$

where $\aleph_{\omega_j}$ denotes the number of finite elements associate with the jth node.

Now we consider matrices L and J. From (2.12) and (2.32) we know the matrix L on the domain edge of the reference element $\hat{\mathcal{K}}$ is a 3×3 diagonal matrix given by

$$\hat{L} = diag\Big(\frac{1}{6}, \frac{1}{6}, \frac{2}{3}\Big), \tag{3.25}$$

and we have

$$\lambda(L) \geqslant \min_j L_{jj}, \tag{3.26}$$

or

$$\lambda(L) \geqslant \frac{1}{3}, \tag{3.27}$$

for the mesh shown in Fig. 3.2.

The matrix J on the domain edge of the reference element $\hat{\mathcal{K}}$ is given by

$$\hat{J} = \begin{bmatrix} \frac{7}{6} & -\frac{1}{6} & -\frac{4}{3} \\ -\frac{1}{6} & \frac{7}{6} & -\frac{4}{3} \\ -\frac{4}{3} & -\frac{4}{3} & \frac{8}{3} \end{bmatrix}, \tag{3.28}$$

so the maximal eigenvalue of $\hat{J}$ is $\lambda_{max}(\hat{J}) = 4$. Similarly we have

$$\lambda(J) \leqslant \lambda_{max}(\hat{J}) \max \aleph_{\tilde{\omega}_j}, \tag{3.29}$$

where $\aleph_{\tilde{\omega}_j}$ denotes the number of line elements associated with the jth node on the domain boundary $\partial\Omega$.

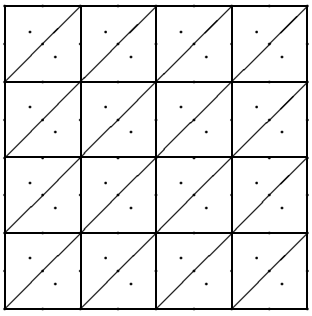

Fig. 3.2. Schematic mesh used in numerical computations. Points denote interpolation nodes. There are seven nodes on each element.

When the computational mesh is fixed, the values of $\max \aleph_{\omega_j}$ and $\max \aleph_{\tilde{\omega}_j}$ can be obtained easily. For example, for the typical uniform mesh shown in Fig. 3.2 or the mesh with the same topological structure as Fig. 3.2, we have

$$\max \aleph_{\omega_j} = 6, \tag{3.30}$$

since there are six triangular elements around the triangular vertex at most, and

$$\max \aleph_{\tilde{\omega}_j} = 2, \tag{3.31}$$

since there are two line elements for a node on the domain boundary at most. Thus from (3.16), (3.21), (3.24) and (3.30), we can get the stability condition for the Dirichlet condition and the first-order ABCs

$$\Delta t \leqslant 2\frac{h}{c}\sqrt{\frac{2}{15} \times \frac{1}{6 \times 10.773929}} = \frac{0.0908h}{c}. \tag{3.32}$$

And from (3.17), (3.27), (3.29) and (3.31) we can obtain the stability condition for the second-order ABCs

$$\begin{aligned}\Delta t &\leqslant \frac{h}{c}\min\left\{\sqrt{3\times\frac{2}{15}\times\frac{1}{6\times 10.773929}},\ \sqrt{2\times\frac{1}{3}\times\frac{1}{4\times 2}}\right\}\\ &\leqslant \frac{h}{c}\min\Big\{0.0787,\ 0.2887\Big\}\leqslant\frac{0.0787h}{c}.\end{aligned}\tag{3.33}$$

Therefore, we have the following theorem:

Theorem 3.2. *For the typical uniform mesh shown in Fig.* 3.2 *or the mesh with the same topology as Fig.* 3.2*, the stability condition is*

$$\Delta t\leqslant\frac{0.0908h}{c},\tag{3.34}$$

for the Dirichlet condition and the first-order ABCs. Moreover, the stability condition is

$$\Delta t\leqslant\frac{0.0787h}{c},\tag{3.35}$$

for the second-order ABCs.

Remarks: For the general unstructural mesh, the similar results like (3.34) and (3.35) can also be obtained based on the idea above. For the inhomogeneous media, we may consider velocity $c(x,z)$ as the maximal value of velocity. It is obvious that the stability condition for the second-order ABCs is more strict than the stability condition for the first-order ABCs.

4. Numerical Computations

First of all, we present a comparison between the finite element approximation and the exact solution. For simplicity, we set $c(x,z)=1$. The exact solution is chosen as

$$u(x,z,t)=\sin\Big(\frac{\pi x}{10}\Big)\sin\Big(\frac{\pi z}{10}\Big)\sin(t^2),\tag{4.1}$$

which produces a source term $s(x,z,t)$ on the right hand side of (2.1):

$$s(x,z,t)=\sin\Big(\frac{\pi x}{10}\Big)\sin\Big(\frac{\pi z}{10}\Big)\Big(2\frac{\pi^2}{100}\sin(t^2)+2\cos(t^2)-4t^2\sin(t^2)\Big).\tag{4.2}$$

The computational domain Ω is $(x,z)=[0,10]\times[0,10]$. Fig. 4.1 is a comparison of vibration waveform between the finite element solution (dashed) and the exact solution (solid) at a fixed position $(x,z)=(5.0,5.0)$. We can see that the two vibration curves coincide very well. We also numerically test the convergence rate of the third-order Lagrange element. We consider L_2 norm after some fixed propagation time, for example $0.1s$. We choose different mesh size h but keep the ratio $\Delta t/h$ be constant 0.002. Fig. 4.2 is the log-log plot of the errors. The circles represent the errors and line represents the least-square fitted line. We found that the slope of the line is 3.02 which shows perfect agreement between theory and computations of convergence order. By the way we point out that the chose of the fixed propagation time has no effect on the convergence analysis.

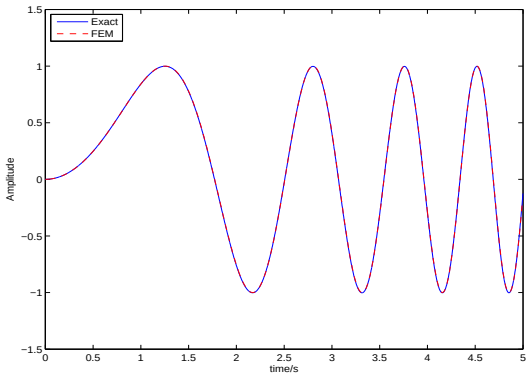

Fig. 4.1. A comparison between the finite element solution (dashed) and the exact solution (solid). Both curves coincide very well.

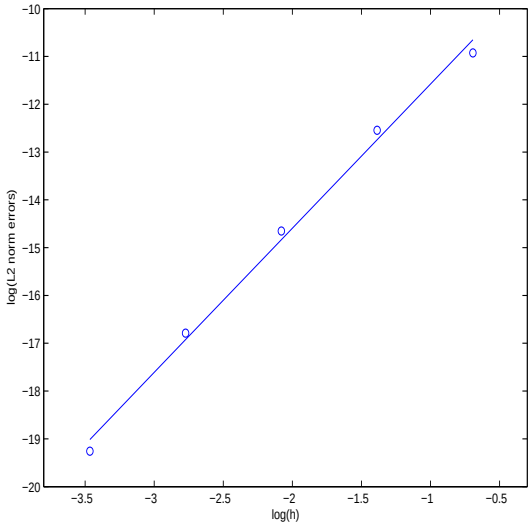

Fig. 4.2. A log-log plot for the L_2 norm errors.

In the following, we consider wave simulation with ABCs. The initial conditions in the computations are zero. For simplicity, we consider a homogeneous model temporary. The velocity is $c(x,z) = 1000m/s$. The simulation domain is a square and is meshed by right-angle triangles like Fig. 3.2. The time signature of the source is

$$f(t) = \begin{cases} -2\pi^2 f_0(t-t_0)e^{-\pi^2 f_0^2(t-t_0)}, & t \leqslant 2t_0, \\ 0, & t > 2t_0, \end{cases} \tag{4.3}$$

where $t_0 = 1/f_0$, and f_0 is the central frequency and is chosen 20Hz. The space distribution of the source is given by the function

$$g(x,z) = e^{-a[(x-x_0)^2+(z-z_0)^2]^{1/2}}, \tag{4.4}$$

where (x_0, z_0) is the source position, and a is a suitable constant which we choose $a = 10$ in our computations. We choose $h = 5m$. The explicit expressions (3.34) and (3.35) can be applied directly in numerical computations. From (3.34) and (3.35) we know that the stability condition

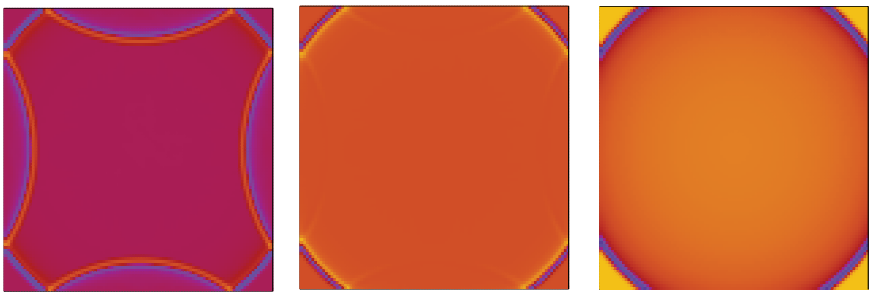

(a) (b) (c)

Fig. 4.3. Snapshots of wave propagation in a homogeneous model at 1.5s with the Dirichlet condition (a), the first-order (b) and second-order (c) ABCs.

is $\Delta t \leq 0.000454s$ for the Dirichlet condition and the first-order ABCs, and $\Delta t \leq 0.0003935s$ for the second-order ABCs. For the sake of comparison the time step is chosen $0.0001s$. Fig. 4.3 shows the snapshots of wave propagation at 1.5s with the Dirichlet condition (a), the first-order (b) and second-order (c) ABCs. As we can see in Fig. 4.3(a) the boundary reflections are serious before absorption but they are eliminated effectively after adding ABCs. Comparisons in Fig. 4.3 show that both the first-order and second-order ABCs can absorb boundary reflections well, and that the second-order ABCs (c) behaviors a little better than the first-order ABCs (b) for this model. The ratio of cpu time between two cases with the first-order and second-order ABCs is about 1:2. We also give a comparison of computational time to show the necessity of using mass-lumping technique. The cpu time for extrapolating every 100 time steps is 10.3s if the mass-lumping technique is used in the computations, while it is 3h41m if it is not. This cpu comparison is obtained on a PC with one processor and 3Ghz frequency.

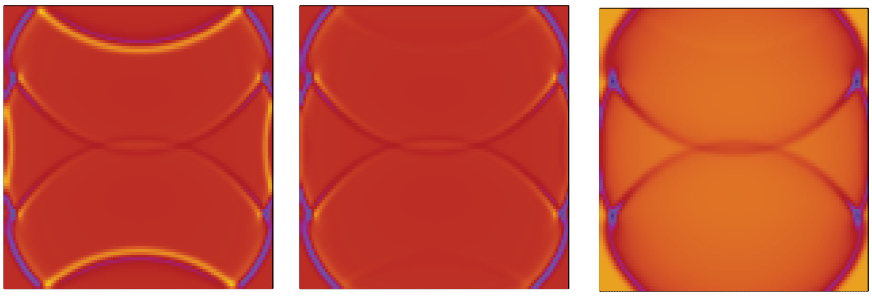

(a) (b) (c)

Fig. 4.4. Snapshots of wave propagation in a three-layered model at 0.88s with the Dirichlet condition (a), the first-order (b) and second-order (c) ABCs.

The next numerical example is a three-layered model with interval velocity $2100m/s$, 1500 m/s and $2200m/s$ from top to bottom respectively. We choose $h = 12m$ in computations. From (3.34) and (3.35) we know that the stability condition is $\Delta t \leq 0.0004953s$ for the Dirichlet condition and the first-order ABCs, and $\Delta t \leq 0.0004293s$ for the second-order ABCs. We still choose $\Delta t = 0.0001s$ for comparison. Fig. 4.4 shows the snapshots of wave propagation at 0.88s with the Dirichlet condition (a), the first-order (b) and second-order (c) ABCs. Comparisons in Fig. 4.4 show that the boundary reflections are absorbed obviously after using the first-order

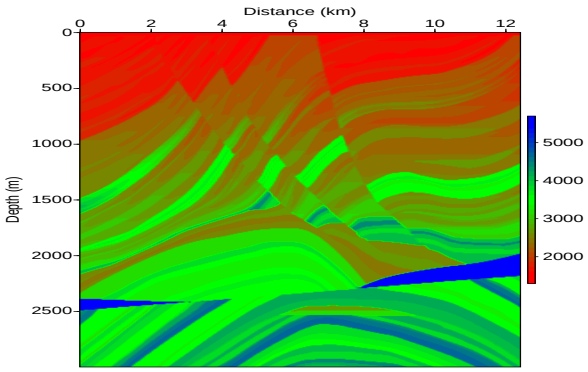

Fig. 4.5. Marmousi velocity model.

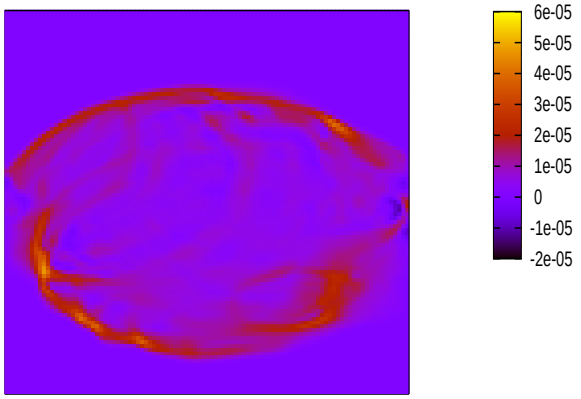

Fig. 4.6. Snapshot of wave propagation in Marmousi model at 0.9s with the Dirichlet condition.

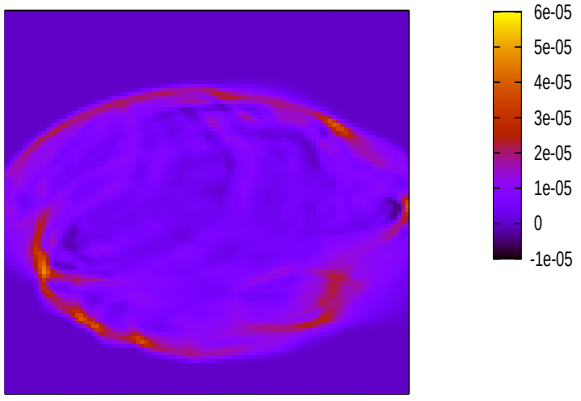

Fig. 4.7. Snapshot of wave propagation in Marmousi model at 0.9s with the first-order ABCs.

or the second-order ABCs.

Finally we select the complex Marmousi model which is shown in Fig. 4.5. The velocity varies from $1500m/s$ to $5500m/s$. The model is gridded with $(N_x, N_z) = 490 \times 750$. The Marmousi model is usually used for testing the ability of migration/inversion algorithms (see,

e.g., [48, 50, 51]). Here we use it to simulate wave propagation. The source position is set at the grid $(x_i, z_i) = (250, 350)$ of the model. We choose mesh size $h = 10m$ in computations. From (3.34) and (3.35) we know the stability is $\Delta t \leq 0.0001651s$ for the Dirichlet condition and the first-order ABCs, and $\Delta t \leq 0.0001431s$ for the second-order ABCs. We choose the time step $\Delta t = 0.0001s$. The total degrees are 2200043. The cpu time for extrapolating every 100 time steps is about one minute. Fig. 4.6 shows the snapshot of the waves at 0.9s with the Dirichlet condition, and Fig. 4.7 is the result for the first-order ABCs. The result for the second-order ABCs is much more similarly with Fig. 4.7 for this model. We omit it here to save space. Comparing Fig. 4.7 with Fig. 4.6, we can see the boundary reflections in Fig. 4.6 are eliminated effectively in Fig. 4.7.

5. Conclusions

The simulation of wave propagation has important applications in oil prospection and geophysical inverse problem. To provide an efficient and accurate solver for these problems, we have proposed a new discretization form for the wave equation and numerically verified its corresponding finite element method on triangular mesh with the third-order Lagrange element for wave simulations. The adopted element may keep the mass lumping technique. The approach allows us to naturally impose the first-order and the second-order absorbing boundary conditions, which are essential for simulation in practical situations. This approach makes us to be easier to construct high accuracy schemes for the absorbing boundary conditions. Moreover, new stability conditions both in abstract and explicit forms for the full-discrete the schemes are derived which are very useful for designing computational parameters. Numerical results show that our method is very efficient and produces numerical solutions with negligible artificial boundary reflections. The new idea of stability analysis in this paper can be applied to other similar problems. For the irregular and curved domain boundary we may adopt the perfectly matched layer method, which is our future research topic.

Acknowledgments. The authors are grateful to the anonymous referees for their helps and constructive comments which have improved the paper much. We also thank the funding from the National Center for Mathematics and Interdisciplinary Sciences in Academy of Mathematics and Systems Science, Chinese Academy of Sciences. This research is supported by the State Key Project with grant number 2010CB731505.

References

[1] K.A. Atkinson, An Introduction to Numerical Analysis (2nd ed.), John Wiley and Sons, 1989.
[2] R.M. Alford, K.R. Kelly and D.M. Boore, Accuracy of finite-difference modeling of the acoustic wave equations, *Geophysics*, **39** (1974), 834-842.
[3] B.A. Auld, Acoustic Field and Elastic Wave in Solids, Volume I and II, Wiley, 1973.
[4] R.E. Bank and L.R. Scott, On the conditioning of finite element equations with highly refined meshes, *SIAM J. Numer. Anal.*, **26** (1989), 1383-1394.
[5] J.P. Bérenger, A perfectly matched layer for the absorption of electromagnetic waves, *J. Comput. Phys.*, **114** (1994), 185-200.
[6] J.M. Carcione, D. Kosloff, A. Behle and G. Seriani, A spectral scheme for wave propogation simulation in 3-D elastic-anisotropic media, *Geophysics*, **57** (1992), 1593-1607.

[7] C. Cerjan, D. Kosloff, R. Kosloff and M. Reshef, A non-reflecting boundary condition for discrete acoustic and elastic wave equation, *Geophysics*, **50** (1985), 705-708.
[8] H. Chan, E.T. Chung and G. Cohen, Stability and dispersion analysis of the staggered discontinuous Galerkin method for wave propagation, *Int. J. Numer. Anal. Model.*, **10** (2013), 233-256.
[9] E.T. Chung and P. Ciarlet, A staggered discontinuous Galerkin method for wave propagation in media with dielectrics and meta-materials, *J. Comput. Appl. Math.*, **239** (2013), 189-207.
[10] E.T. Chung, P. Ciarlet and T. Yu, Convergence and superconvergence of staggered discontinuous Galerkin methods for the three-dimensional Maxwell's equations on Cartesian grids, *J. Comput. Phys.*, **235** (2013), 14-31.
[11] E.T. Chung, Q. Du and J. Zou, Convergence analysis on a finite volume method for Maxwell's equations in non-homogeneous media, *SIAM J. Numer. Anal.*, **41** (2003), 37-63.
[12] E.T. Chung, Y. Efendiev and R.L. Gibson JR., An energy-conserving discontinuous multiscale finite element method for the wave equation in heterogeneous media, *Advances in Adaptive Data Analysis*, **3** (2011), 251-268.
[13] E.T. Chung and B. Engquist, Convergence analysis of fully discrete finite volume methods for Maxwell's equations in nonhomogeneous media, *SIAM J. Numer. Anal.*, **43** (2005), 303-317.
[14] E.T. Chung and B. Engquist, Optimal discontinuous Galerkin methods for wave propagation, *SIAM J. Numer. Anal.*, **44** (2006), 2131-2158.
[15] E.T. Chung and B. Engquist, Optimal discontinuous Galerkin methods for the acoustic wave equation in higher dimensions, *SIAM J. Numer. Anal.*, **47** (2009), 3820-3848.
[16] R. Clayton and B. Engquist, Absorbing boundary conditions for acoustic and elastic wave equations, *Bulletin of the Seismological Society of America*, **67** (1977), 1529-1540.
[17] G. Cohen, P. Joly, J.E. Roberts and N. Tordjman, Higher order triangular finite elements with mass lumping for the wave equation, *SIAM J. Numer. Anal.*, **38** (2001), 2047-2078.
[18] G. Cohen, Higher-order Numerical Methods for Transient Wave Equations, Springer, 2002.
[19] F. Collino and C. Tsogka, Application of the perfectly matched absorbing layer model to the linear elastodynamic problem in anisotropic heterogeneous media, *Geophysics*, **66** (2001), 294-307.
[20] M.A. Dablain, The application of high–order differencing to the scalar wave equation, *Geophysics*, **51** (1986), 54-66.
[21] Q. Du, D. Wang and L. Zhu, On mesh geometry and stiffness matrix conditioning for general finite element spaces, *SIAM J. Numer. Anal.*, **47** (2009), 1421-1444.
[22] B. Engquist and A. Majda, Absorbing boundary conditions for the numerical simulation of waves, *Math. Comp.*, **31** (1977), 629-651.
[23] I. Fried, Condition of finite element matrices generated from nonuniform meshes, *AIAA Journal*, **10** (1972), 219-221.
[24] I. Fried, Bounds on the extremal eigenvalues of the finite element stiffness and mass matrices and their spectral condition number, *Journal of Sound and Vibration*, **22** (1972), 407-418.
[25] R.L. Higdon, Absorbing boundary conditions for difference approximations to the multidimensional wave equation, *Math. Comp.*, **47** (1986), 437-459.
[26] R.L. Higdon, Numerical absorbing boundary conditions for the wave equation, *Math. Comp.*, **49** (1987), 65-90.
[27] N. Hu, X.Z. Guo and I.N. Katz, Bounds for eigenvalues and condition numbers in the p-version of the finite element method, *Math. Comp.*, **67** (1998), 1423-1450.
[28] D. Komatitsch and J. Tromp, Introduction to the spectral element method for three-dimensional seismic wave propagation, *Geophys. J. Internat.*, **139** (1999), 806-822.
[29] D. Komatitsch, C. Barnes and J. Tromp, Simulation of anisotropic wave propagation based upon a spectral element method, *Geophysics*, **65** (2000), 1251-1260.
[30] D.D. Kosloff and E. Baysal, Forward modeling by a Fourier method, *Geophysics*, **47** (1982), 1402-1412.
[31] D. Kosloff, M. Reshef and D. Loewenthal, Elastic wave calculations by the Fourier method, *Bulltin*

of the Seismological Society of America, **74** (1984), 875-891.

[32] A.R. Levander, Fourth-order finite-difference P-SV seismograms, *Geophysics*, **53** (1988), 1425-1436.

[33] K.J. Marfurt, Accuracy of finite-difference and finite-element modeling of the scalar and elastic wave equations, *Geophysics*, **49** (1984), 533-549.

[34] E.T. Olsen and Jr. J. Douglas, Bounds on spectral condition numbers of matrices arising in the p-version of the finite element method, *Numer. Math.*, **69** (1995), 333-352.

[35] A.T. Patera, A spectral element method for fluid dynamics: Laminar flow in a channel expansion, *J. Comput. Phys.*, **54** (1984), 468-488.

[36] A. Sei, A family of numerical schemes for the computation of elastic waves, *SIAM J. Sci. Comput.*, **16**) (1995), 898-916.

[37] W.D. Smith, A nonreflecting plane boundary for wave propagation problems, *J. Comput. Phys.*, **15** (1974), 492-503

[38] G. Strang and G.J. Fix, An Analysis of the Finite Element Method, Prentice-Hall, Englewood Cliffs, NJ, 1973.

[39] H. Tal-Ezer, D. Kosloff and Z. Koren, An accurate scheme for seismic forward modeling, *Geophys. Prosp.*, **35** (1987), 479-490.

[40] E. Tessmer and D. Kosloff, 3-D elastic modeling with surface tomography by a Chebychev spectral method, *Geophysics*, **59** (1994), 464-473.

[41] E. Tessmer, D. Kessler, D. Kosloff and A. Behle, Multi-domain Chebyshev-Fourier method for the solution of the equations of motion of dynamic elasticity, *J. Comput. Phys.*, **100** (1992), 355-363.

[42] A. Vafidis, F. Abramovici and E.R. Kanasewich, Elastic wave propagation using fully vectorized high order finite-difference algorithms, *Geophysics*, **57** (1992), 218-232.

[43] J. Virieux, P-SV wave propagation in heterogeneous media: velocity-stress finite-difference method, *Geophysics*, **51** (1986), 889-901.

[44] A.J. Wathen, Realistic eigenvalue bounds for the Galerkin mass matrix, *IMA Journal of Numerical Analysis*, **7** (1987), 449-457.

[45] L. Wang and X. Xu, The Mathematical Foundations of the Finite Element Method. Science Press, Beijing (in Chinese), 2004.

[46] G. Zhang, High order approximation of one-way wave equations, *J. Comp. Math.*, **3** (1985), 90-97.

[47] G. Zhang, Coupled equations of wave equation for upgoing and downgoing wave, *Acta Applied Maths.*, **16** (1993), 251-263.

[48] G. Zhang and W. Zhang, Methods for wave equation prestack depth migration, *Science in China Series A-Mathematics, Supp.*, **47** (2004), 111-120.

[49] J. Zhang and D.J. Verschuur, Elastic wave propagation in heterogeneous anisotropic media using the lumped finite-element method, *Geophysics*, **67** (2002), 625-638.

[50] W. Zhang and G. Zhang, 3D hybrid depth migration and four-way splitting schemes, *J. Comput. Math.*, **24** (2006), 463-474.

[51] W. Zhang and Y. Wong, Efficient parallel hybrid computations for three-dimensional wave equation prestack depth imaging, *International Journal of Numerical Aanlysis and Modeling*, **7** (2010), 373-391.

[52] W. Zhang, L. Tong and E.T. Chung, A new high accuracy locally one-dimensional scheme for the wave equation, *J. Comput. Appl. Math.*, **236** (2011), 1343-1353.

[53] W. Zhang, L. Tong and E.T. Chung, Efficient simulation of wave propagation with implicit finite difference schemes, *Numer. Math. Theor. Meth. Appl.*, **5** (2012), 205-228.

[54] O.C. Zienkiewicz and R.L. Taylor, The Finite Element Methods, Volume 1, 5th ed, Elsevier (Singapore) Pte Ltd, 2005.